# Measurement of $^{13}C^{\alpha}-^{13}C^{\beta}$ Dipolar Couplings in $^{15}N,^{13}C,^{2}H$-Labeled Proteins: Application to Domain Orientation in Maltose Binding Protein

**Johan Evenäs, Anthony Mittermaier, Daiwen Yang, and Lewis E. Kay***

*Contribution from the Protein Engineering Network Centres of Excellence and the Departments of Medical Genetics, Biochemistry and Chemistry, University of Toronto, Toronto, Ontario, Canada M5S 1A8*

*Received October 31, 2000. Revised Manuscript Received January 16, 2001*

**Abstract:** TROSY-based HN(CO)CA 2D and 3D pulse schemes are presented for measurement of $^{13}C^{\alpha}-^{13}C^{\beta}$ dipolar couplings in high molecular weight $^{15}N,^{13}C,^{2}H$-labeled proteins. In one approach, $^{13}C^{\alpha}-^{13}C^{\beta}$ dipolar couplings are obtained directly from the time modulation of cross-peak intensities in a set of 2D $^{15}N-^{1}HN$ correlated spectra recorded in both the presence and absence of aligning media. In a second approach 3D data sets are recorded with $^{13}C^{\alpha}-^{13}C^{\beta}$ couplings encoded in a frequency dimension. The utility of the experiments is demonstrated with an application to an $^{15}N,^{13}C,^{2}H$-labeled sample of the ligand free form of maltose binding protein. A comparison of experimental dipolar couplings with those predicted from the X-ray structure of the apo form of this two-domain protein establishes that the relative orientation of the domains in solution and in the crystal state are very similar. This is in contrast to the situation for maltose binding protein in complex with $\beta$-cyclodextrin where the solution structure can be generated from the crystal state via a 11° domain closure.

## Introduction

In the past several years important methodological developments have greatly facilitated NMR studies of high molecular weight biomolecules.[1,2] The use of $^{15}N,^{13}C,^{2}H$-labeling in concert with sophisticated triple-resonance experiments has significantly decreased the rather stringent molecular weight limitations that in the past have been imposed on studies of proteins and nucleic acids.[3,4] In this context new labeling strategies including selective labeling of polypeptide segments with intein-methodology[5,6] and selective protonation in highly deuterated, $^{15}N,^{13}C$-labeled samples[3] have been important. Another recent and significant advance has been the exploitation of the relaxation interference between dipolar and chemical shift anisotropy (CSA) interactions, known as the TROSY effect, leading to significant improvements in sensitivity for many NMR experiments, particularly when recorded at high magnetic fields.[7,8] By using the TROSY principle, high-sensitivity 4D triple resonance experiments were recorded on a sample of maltose binding protein (MBP) in complex with $\beta$-cyclodextrin (rotational correlation time of 46 ns at 5 °C).[9,10] More recently, Wüthrich and co-workers have obtained the backbone assignment and secondary structure for the octameric 110 kDa protein, 7,8-dihydroneopterin aldolase, from *Staphylococcus aureus*[11] using TROSY-type triple resonance 3D experiments.[12,13]

An additional important advance has been the emergence of dipolar couplings as a source of structural[14,15] and potentially dynamic information.[16] These couplings can be measured from fractionally aligned molecules dissolved in a dilute solution of aligning media.[17] With the proper choice of liquid crystalline medium, including phospholipid bicelles[17] or phage,[18,19] an appropriate degree of alignment can be obtained for many proteins with little decrease in spectral quality.[20,21] Dipolar couplings report on the orientation of dipolar vectors relative to the molecular alignment frame. These long-range restraints are highly complementary to short-range NOE-derived distance restraints, and their use in structural studies of large highly deuterated proteins is particularly important since the number

(1) Bax, A. *Curr. Opin. Struct. Biol.* **1994**, *4*, 738−744.
(2) Wider, G.; Wüthrich, K. *Curr. Opin. Struct. Biol.* **1999**, *9*, 594−601.
(3) Gardner, K. H.; Kay, L. E. *Annu. Rev. Biophys. Biomol. Struct.* **1998**, *27*, 357−406.
(4) Farmer, B. T.; Venters, R. A. *NMR of perdeuterated large proteins*; Krishna, N. R., Berliner, L. J., Eds.; Kluwer Academic/Plenum Publishers: New York, 1998; Vol. 16, pp 75−120.
(5) Yamazaki, T.; Otomo, T.; Oda, N.; Kyogoku, Y.; Uegaki, K.; Ito, K.; Ishino, Y.; Nakamura, H. *J. Am. Chem. Soc.* **1998**, *120*, 5591−5592.
(6) Xu, R.; Ayers, B.; Cowburn, D.; Muir, T. W. *Proc. Natl. Acad. Sci. U.S.A.* **1999**, *96*, 388−93.
(7) Pervushin, K.; Riek, R.; Wider, G.; Wüthrich, K. *Proc. Natl. Acad. Sci. U.S.A.* **1997**, *94*, 12366−12371.
(8) Pervushin, K.; Riek, R.; Wider, G.; Wüthrich, K. *J. Am. Chem. Soc.* **1998**, *120*, 6394−6400.
(9) Yang, D.; Kay, L. E. *J. Am. Chem. Soc.* **1999**, *121*, 2571−2575.
(10) Konrat, R.; Yang, D.; Kay, L. E. *J. Biomol. NMR* **1999**, *15*, 309−313.
(11) Salzmann, M.; Pervushin, K.; Wider, G.; Senn, H.; Wuthrich, K. *J. Am. Chem. Soc.* **2000**, *122*, 7543−7548.
(12) Pervushin, K. V.; Wider, G.; Riek, R.; Wüthrich, K. *Proc. Natl. Acad. Sci. U.S.A.* **1999**, *96*, 9607−9612.
(13) Salzmann, M.; Wider, G.; Pervushin, K.; Senn, H.; Wuthrich, K. *J. Am. Chem. Soc.* **1999**, *121*, 844−848.
(14) Tjandra, N.; Omichinski, J. G.; Gronenborn, A. M.; Clore, G. M.; Bax, A. *Nature Struct. Biol.* **1997**, *4*, 732−738.
(15) Tolman, J. R.; Flanagan, J. M.; Kennedy, M. A.; Prestegard, J. H. *Proc. Natl. Acad. Sci. U.S.A.* **1995**, *92*, 9279−9283.
(16) Tolman, J. R.; Flanagan, J. M.; Kennedy, M. A.; Prestegard, J. H. *Nature Struct. Biol.* **1997**, *4*, 292−297.
(17) Tjandra, N.; Bax, A. *Science* **1997**, *278*, 1111−1114.
(18) Hansen, M. R.; Mueller, L.; Pardi, A. *Nature Struct. Biol.* **1998**, *5*, 1065−1074.
(19) Clore, G. M.; Starich, M. R.; Gronenborn, A. M. *J. Am. Chem. Soc.* **1998**, *120*, 10571−10572.
(20) Prestegard, J. H. *Nature Struct. Biol. NMR Suppl.* **1998**, *5*, 517−522.
(21) Bax, A.; Tjandra, N. *J. Biomol. NMR* **1997**, *10*, 289−292.

10.1021/ja003833y CCC: $20.00 
Published on Web 02/27/2001

of NOE cross-peaks is significantly diminished relative to fully protonated molecules.[22,23] In this regard we have recently developed a labeling strategy in which $^{15}N$,$^{13}C$, and highly deuterated proteins are produced with protonation at methyl sites of Val, Leu, and Ile ($\delta 1$ only) residues.[24,25] Methyl−methyl, methyl−HN, and HN−HN NOEs can be recorded to generate low-resolution global folds of proteins which are subsequently refined by using a set of five planar dipolar coupling restraints/peptide.[23] It would be of considerable interest to extend the measurement of dipolar couplings in highly deuterated proteins to include those outside the peptide plane. The one-bond $C^{\alpha}-C^{\beta}$ dipolar coupling, $^1D_{C\alpha C\beta}$, is a particularly good candidate as the $C^{\alpha}-C^{\beta}$ bond provides a bridge between the protein backbone and the side chain and, in concert with previously measured $^1D_{NHN}$, $^1D_{NCO}$, $^1D_{COCA}$, $^2D_{HNCO}$, and $^3D_{HNCA}$ dipolar couplings,[26] $^1D_{C\alpha C\beta}$ helps constrain the backbone dihedral angle $\psi$. While methods for measurement of $^1J_{C\alpha C\beta}$ and $^1D_{C\alpha C\beta}$ have been reported previously,[27,28] applications have focused on the small protein ubiquitin (~9 kDa)[27,28] and it is not clear a priori whether $^1D_{C\alpha C\beta}$ couplings can be extracted from proteins with molecular weights on the order of 40 kDa. In this report we describe experiments for measuring $^1D_{C\alpha C\beta}$ in high molecular weight deuterated proteins and present an application to the unligated form of MBP (41 kDa). A comparison of the measured dipolar couplings with those predicted from the X-ray structure of this two-domain protein establishes that, in contrast to the $\beta$-cyclodextrin loaded form of the molecule,[29] the domain orientation for the unligated protein in both X-ray and solution states is similar.

## Materials and Methods

$^{15}N$,$^{13}C$,$^2H$-labeled apo-MBP was prepared as described previously[30] but without $\beta$-cyclodextrin and without selective protonation of methyl groups. Samples comprised of 1.4 mM protein (no phage) or 1.1 mM protein (phage), 20 mM sodium phosphate buffer (pH 7.2), 3 mM $NaN_3$, 0.1 mM EDTA, 50 $\mu$M Pefabloc, and 10% $D_2O$ were used for all spectra recorded. Sample alignment was obtained by adding Pf1 phage[18] to a concentration of ~18 mg/mL ($^2H$ $D_2O$ splitting of 18 Hz). NMR experiments were recorded on a Varian Inova 600 MHz spectrometer with data processing performed with NMRPipe/NMRDraw software.[31] $^1HN$, $^{15}N$, $^{13}C^{\alpha}$, and $^{13}C^{\beta}$ chemical shift assignments of apo-MBP (to be presented elsewhere) were obtained by using 3D constant-time triple resonance methodology[32−34] (no phage sample) with all experiments employing the TROSY principle (see the Supporting Information of Yang and Kay[9]). The $^1HN$ and $^{15}N$ chemical shifts of 14 residues in the protein remain unassigned; in many cases this is the result of extreme peak broadening due to chemical exchange processes. Predicted values of dipolar couplings were generated by using in-house software, Conformist1.0,[29] written in MATLAB (MathWorks Inc.) format.

**2D $^1D_{C\alpha C\beta}$-HN(CO)CA Method.** Eight 2D data sets were recorded as a function of $^{13}C^{\alpha}-^{13}C^{\beta}$ coupling evolution time, $2T_C$ (Figure 1). Data sets were obtained for $2T_C$ values of 0.1, 7.4, 14.7, 22.0, 29.4, 36.8, 44.0, and 51.4 ms for samples with and without phage. Each 2D spectrum was acquired as a complex data matrix of 110 × 576 points ($t_2$, $t_3$) corresponding to $^{15}N$ and $^1HN$ acquisition times of 67 and 64 ms, respectively. 64 and 80 transients were acquired/FID for the isotropic and oriented sample, respectively, with a relaxation delay of 1.5 s, resulting in net acquisition times for each series of 53 and 67 h. The data sets were processed by using sine-squared window functions shifted by 81° and 63° in the $^{15}N$ and $^1HN$ dimensions, respectively. The final 2D spectra consisted of 512 × 709 real points after zero-filling and retaining only the region with cross-peaks. Cross-peak intensities were extracted by using the nlinLS feature of NMRPipe.[31] Values of $^{13}C^{\alpha}-^{13}C^{\beta}$ couplings (scalar or scalar + dipolar) were extracted from the time domain modulation of cross-peak intensities by using a nonlinear fitting program written in MATLAB (MathWorks Inc.). Experimental uncertainties were obtained by using the jack-knife procedure[35] where each of the eight data points is removed in turn and a new coupling value obtained. The standard deviation in the eight values obtained for each coupling is taken as the error in the measurement.

**3D $^1D_{C\alpha C\beta}$-HN(CO)CA Method.** 3D data sets were acquired as matrices consisting of (64, 32, 576) complex points in the ($^{13}C^{\alpha}$, $^{15}N$, $^1HN$) dimensions, corresponding to acquisition times of (27.4 ms, 18.9 ms, 63.9 ms). 8 (no phage) and 16 (phage) scans/FID were acquired along with a relaxation delay of 1.1 s giving rise to net acquisition times of 24 (no phage) and 47 h (phage), respectively. Briefly, each 3D data set was processed by using a sine-squared window function shifted by 63° in the $^1HN$ dimension and a sine window shifted by 81° in the $^{13}C^{\alpha}$ dimension. The $^{15}N$ time domain was doubled by mirror-image linear prediction[36] prior to the application of a sine-squared window function shifted by 79°. After zero-filling the final data sets comprised (512, 128, 399) real points, corresponding to a digital resolution of (4.5 Hz/pt, 12.8 Hz/pt, 3.9 Hz/pt). The spectra were analyzed by using the PIPP/CAPP[37] suite of programs.

## Results and Discussion

Figure 1 presents the 2D (a) and 3D (b) HN(CO)CA-based[33,38] triple-resonance experiments that have been used to measure the one-bond $^{13}C^{\alpha}-^{13}C^{\beta}$ dipolar couplings in $^{15}N$,$^{13}C$,$^2H$-labeled unligated MBP. Since related pulse schemes have been discussed previously in the literature only a very brief description of the sequences is presented here, highlighting the unique features of the present experiments. The magnetization flow during the course of each of the experiments can be described by

$$\mathrm{HN} \xrightarrow{{}^1\boldsymbol{J}_{NH}} {}^{15}\mathrm{N} \xrightarrow{{}^1\boldsymbol{J}_{NCO}} {}^{13}\mathrm{CO} \xrightarrow{{}^1\boldsymbol{J}_{COC\alpha}} {}^{13}\mathrm{C}^{\alpha} \xrightarrow{{}^1\boldsymbol{J}_{COC\alpha}} {}^{13}\mathrm{CO} \xrightarrow{{}^1\boldsymbol{J}_{NCO}} {}^{15}\mathrm{N}\,(t_2) \xrightarrow{{}^1\boldsymbol{J}_{NH}} \mathrm{HN}\,(t_3) \quad (1)$$

where the active couplings responsible for each transfer step are indicated above each arrow and the bold faced, italicized $^1\boldsymbol{J}_{ij}$ denotes the sum of the dipolar, $^1D_{ij}$, and scalar, $^1J_{ij}$, couplings. Both pulse schemes employ the TROSY principle in the $^{15}N$ and $^1HN$ dimensions, implemented as described previously to minimize relaxation losses during the $^{15}N$ →

(22) Clore, G. M.; Starich, M. R.; Bewley, C. A.; Cai, M.; Kuszewski, J. *J. Am. Chem. Soc.* **1999**, *121*, 6513−6514.
(23) Mueller, G. A.; Choy, W. Y.; Yang, D.; Forman-Kay, J. D.; Venters, R. A.; Kay, L. E. *J. Mol. Biol.* **2000**, *300*, 197−212.
(24) Gardner, K. H.; Kay, L. E. *J. Am. Chem. Soc.* **1997**, *119*, 7599−7600.
(25) Goto, N. K.; Gardner, K. H.; Mueller, G. A.; Willis, R. C.; Kay, L. E. *J. Biomol. NMR* **1999**, *13*, 369−374.
(26) Yang, D.; Venters, R. A.; Mueller, G. A.; Choy, W. Y.; Kay, L. E. *J. Biomol. NMR* **1999**, *14*, 333−343.
(27) Cornilescu, G.; Bax, A.; Case, D. A. *J. Am. Chem. Soc.* **2000**, *122*, 2168−2171.
(28) Permi, P.; Rosevar, P. R.; Annila, A. *J. Biomol. NMR* **2000**, *17*, 43−54.
(29) Skrynnikov, N. R.; Goto, N. K.; Yang, D.; Choy, W. Y.; Tolman, J. R.; Mueller, G. A.; Kay, L. E. *J. Mol. Biol.* **2000**, *295*, 1265−1273.
(30) Gardner, K. H.; Zhang, X.; Gehring, K.; Kay, L. E. *J. Am. Chem. Soc.* **1998**, *120*, 11738−11748.
(31) Delaglio, F.; Grzesiek, S.; Vuister, G. W.; Zhu, G.; Pfeifer, J.; Bax, A. *J. Biomol. NMR* **1995**, *6*, 277−293.
(32) Yamazaki, T.; Lee, W.; Revington, M.; Mattiello, D. L.; Dahlquist, F. W.; Arrowsmith, C. H.; Kay, L. E. *J. Am. Chem. Soc.* **1994**, *116*, 6464−6465.
(33) Yamazaki, T.; Lee, W.; Arrowsmith, C. H.; Muhandiram, D. R.; Kay, L. E. *J. Am. Chem. Soc.* **1994**, *116*, 11655−11666.
(34) Shan, X.; Gardner, K. H.; Muhandiram, D. R.; Rao, N. S.; Arrowsmith, C. H.; Kay, L. E. *J. Am. Chem. Soc.* **1996**, *118*, 6570−6579.
(35) Mosteller, F.; Tukey, J. W. *Data Analysis and Regression. A Second Course in Statistics*; Addison-Wesley: Reading, MA, 1977.
(36) Zhu, G.; Bax, A. *J. Magn. Reson.* **1990**, *90*, 405−410.
(37) Garrett, D. S.; Powers, R.; Gronenborn, A. M.; Clore, G. M. *J. Magn. Reson.* **1991**, *95*, 214−220.
(38) Bax, A.; Ikura, M. *J. Biomol. NMR* **1991**, *1*, 99−104.

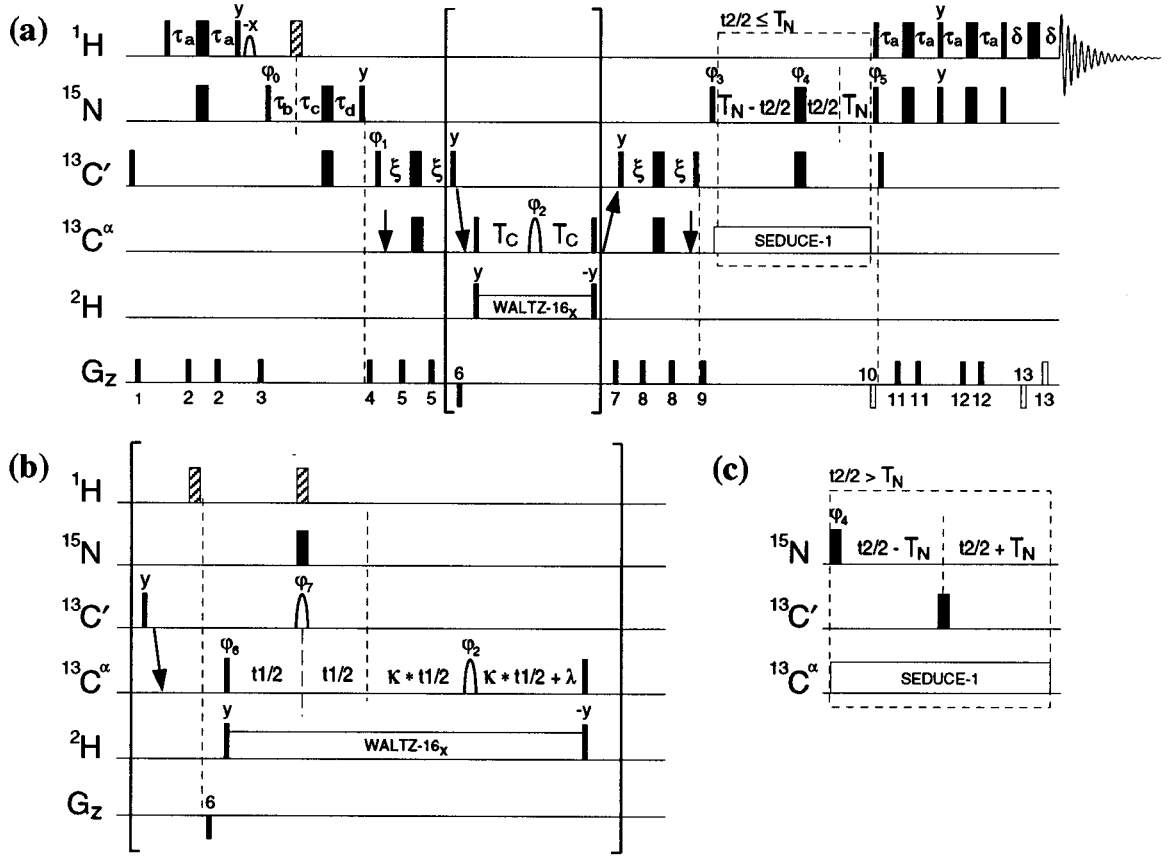


**Figure 1.** 2D (a) and 3D (b) TROSY-based HN(CO)CA pulse schemes to measure one-bond $^{13}C^{\alpha}-^{13}C^{\beta}$ dipolar couplings in $^{15}N$,$^{13}C$,$^{2}H$-labeled proteins. In either the 2D or 3D experiments, a shared constant-time approach[40,41] can be implemented whereby scheme (c) replaces the dash-boxed region of (a) for $t_2/2 > T_N$. In the 3D-experiment the bracketed sequence in (b) replaces the corresponding region in (a). The pulse schemes utilize active suppression of the anti-TROSY component, with careful adjustment of $\varphi_0$ (45°), as described previously.[8,9] All narrow (wide) pulses are applied with flip angles of 90° (180°) along the *x*-axis, unless indicated otherwise. The $^{1}H$, $^{15}N$, and $^{2}H$ carriers are positioned at 4.65 (water), 119, and 4.5 ppm, respectively. The $^{13}C$ carrier is set to 176 ppm, switched to 58 ppm prior to the first $^{13}C^{\alpha}$ 90° pulse, and returned to 176 ppm after the next $^{13}C^{\alpha}$ 90° pulse (indicated by diagonal arrows). $^{1}H$ pulses are applied at a field strength of 32 kHz with the exception of the water selective 90° pulse of duration 1.6 ms. The striped $^{1}H$ pulses are of the composite variety $(90^{\circ}_{x}\,180^{\circ}_{y}\,90^{\circ}_{x})$.[50] All $^{15}N$ pulses employ a 5.5 kHz field. The $^{13}C'$ and $^{13}C^{\alpha}$ rectangular pulses are applied at a field strength of $\Delta/\sqrt{15}$ (90°) or $\Delta/\sqrt{3}$ (180°), where $\Delta$ is the separation in Hz between the centers of the $^{13}C'$ and $^{13}C^{\alpha}$ chemical shift regions.[51] The $^{13}C^{\alpha}$ refocusing pulse of phase $\phi 2$ has the RE-BURP[52] profile (400 $\mu$s centered at 45 ppm) while the selective $^{13}C'$ 180° pulse (240 $\mu$s) of phase $\phi 7$ (b) is applied with the SEDUCE-1 profile.[53] $^{13}C^{\alpha}$ SEDUCE decoupling[54] is achieved by using a 118 ppm cosine-modulated WALTZ-16 field[55] employing SEDUCE-1 pulses (336 $\mu$s 90°). The $^{13}C^{\alpha}$ inversion pulse during the first (second) $2\xi$ period is applied after (before) the $^{13}C'$ 180° refocusing pulse, with the vertical arrows indicating the positions of Bloch−Siegert compensation[56] $^{13}C^{\alpha}$ pulses. The final $^{13}C'$ 90° purge pulse ensures that pure absorptive line shapes are obtained in $F_2$ and $F_3$.[26] All off-resonance $^{13}C$ pulses are generated by phase modulation of the carrier.[57,58] The $^{2}H$ 90° pulses which flank the 0.6 kHz $^{2}H$ WALTZ-16 decoupling element are applied at a field of 2.0 kHz. The delays used are $\tau_a = 2.3$ ms, $\tau_b = 1.34$ ms, $\tau_c = \tau_d - \tau_b$, $\tau_d = 12.0$ ms, $\xi = 4.1$ ms, $T_N = 12.0$ ms, $\delta = 0.25$ ms, and $\kappa = 1.4$. The phase cycling employed (2D) is $\varphi 0 = 45°$, $\varphi 1 = x, -x$; $\varphi 2 = 2(x), 2(y), 2(-x), 2(-y)$; $\varphi 3 = 8(y), 8(-y)$; $\varphi 4 = x, -x$; $\varphi 5 = x$; rec = $x, 2(-x), 2(x), 2(-x), x, -x, 2(x), 2(-x), 2(x), -x$, while for the 3D sequence the phase cycling used is $\varphi 0 = 45°$, $\varphi 1 = x, -x$; $\varphi 2 = 2(x), 2(y), 2(-x), 2(-y)$; $\varphi 3 = y, -y$; $\varphi 4 = 4(x), 4(-x)$; $\varphi 5 = x$; $\varphi 6 = x$; $\varphi 7 = 4(x), 4(-x)$; rec = $2(x), 2(-x)$. Quadrature detection in the $^{13}C^{\alpha}$ dimension (3D experiment) is obtained by States-TPPI[59] of $\varphi 6$. Quadrature in $t_2$ is obtained by using the gradient-enhanced sensitivity method[60,61] in which two separate data sets are recorded for each $t_2$ increment with 180° added to $\varphi 5$ and the sign of gradient 10 inverted for the second set. The phase $\phi 3$ is incremented by 180° in concert with the receiver for each complex $t_2$ point. The duration and the strengths of the gradients used are the following: 1 (0.5 ms, 8 G/cm), 2 (0.5 ms, 4 G/cm), 3 (1 ms, 8 G/cm), 4 (1 ms, 1 G/cm), 5 (1 ms, 7 G/cm), 6 (1 ms, −15000 G/cm), 7 (1 ms, 8 G/cm), 8 (1 ms, 0.4 G/cm), 9 (0.6 ms, 10 G/cm), 10 (1.25 ms, −30 G/cm), 11 (0.5 ms, 8 G/cm), 12 (0.3 ms, 2 G/cm), 13 (0.0625 ms, 28.7 G/cm).

$^{1}$HN transfer prior to detection.[9,39] In both pulse sequences active suppression of the anti-TROSY component is performed as described previously by Pervushin et al.[8] and Yang and Kay[9] (see Supporting Information in this reference).

**2D $^{1}D_{C\alpha C\beta}$-HN(CO)CA Method.** Measurement of $^{13}C^{\alpha}-^{13}C^{\beta}$ dipolar couplings is achieved by using the pulse scheme of Figure 1a,c. After transferring the magnetization from the $^{1}$HN of residue $i$ to the $^{13}C^{\alpha}$ of residue $(i-1)$ via the intervening $^{13}$CO (see eq 1), evolution due to the one-bond coupling, $^{1}J_{C\alpha C\beta}$, occurs during the delay $2T_C$. Subsequently magnetization is transferred back to the $^{15}N$ of residue $i$ ($t_2$) and then to the $^{1}$HN for detection ($t_3$). A series of 2D $^{15}N-^{1}HN$ correlation spectra are recorded as a function of $2T_C$, with evolution of $^{13}C^{\alpha}$ magnetization occurring for a period, $T = 2T_C + pw^{180^{\circ}}_{C\alpha} + \Gamma pw^{90^{\circ}}_{C\alpha}$, where $pw^{180^{\circ}}_{C\alpha}$ is the length of the RE-BURP pulse of phase $\phi 2$ in the middle of the $2T_C$ period and $pw^{90^{\circ}}_{Ca}$ is the length of the $^{13}C^{\alpha}$ 90° pulses bracketing the $2T_C$ period. Numerical simulations have established that $\Gamma \approx (1.5)(4/\pi)$, with the exact value depending on the chemical shifts of $^{13}C^{\alpha}$ and $^{13}C^{\beta}$ spins and $pw^{90^{\circ}}_{C\alpha}$. The variation of $\Gamma$ with offset is small over the region of interest and the error associated with assuming

(39) Yang, D.; Kay, L. E. *J. Biomol. NMR* **1999**, *13*, 3−10.

a constant value is negligible. Cross-peak intensities, $I$, are modulated according to

$$I = \{I_0 \cos(\pi^1 \boldsymbol{J}_{C\alpha C\beta} T) + B\} \exp[-T/T_2^{C\alpha}] \qquad (2)$$

where $I_0 + B$ is the intensity at $T = 0$, and $T_2^{C\alpha}$ is the effective transverse relaxation time for $^{13}C^{\alpha}$, with $B$ an offset term that accounts both for imperfect inversion of $^{13}C^{\beta}$ spins leading to refocusing of $^1\boldsymbol{J}_{C\alpha C\beta}$ evolution and incomplete $^{13}C$ labeling at the $C^{\beta}$ position. A set of 2D experiments is recorded on samples without and with aligning media, and values of $^1J_{C\alpha C\beta}$ and $^1\boldsymbol{J}_{C\alpha C\beta}$ (for residue $i-1$) obtained by fitting the intensity dependence of each cross-peak as a function of $T$ to eq 2. The value of $^1D_{C\alpha C\beta}$ follows directly from $^1D_{C\alpha C\beta} = {}^1\boldsymbol{J}_{C\alpha C\beta} - {}^1J_{C\alpha C\beta}$.

To maximize the number of resolved cross-peaks in the 2D spectra, the $^{15}N$ chemical shift is recorded by using a shared constant-time approach[40,41] with the scheme of Figure 1a employed for $t_2 \leq 2T_N$, modified with the sequence of Figure 1c for $t_2 > 2T_N$. This ensures that antiphase $^{15}N$ magnetization, of the form $2N_xCO_z$, which is present immediately following the $^{15}N$ pulse of phase $\phi 3$, is refocused optimally for a period of $2T_N$, without restricting the time for nitrogen chemical shift evolution in any way.

The left panels of Figure 2 show fits of the experimental data for Leu 139 (a, $^1D_{C\alpha C\beta} = -5.7$ Hz) and Thr 249 (b, $^1D_{C\alpha C\beta} = 4.3$ Hz), with cross-peak intensities measured without and with phage indicated by closed and open circles, respectively. In total 215 scalar couplings could be obtained in the unoriented sample of unligated MBP, with an average $^1J_{C\alpha C\beta}$ value of $34.4 \pm 2.0$ Hz (ranging from 31.3 to 42.4 Hz), where the uncertainty is the calculated standard deviation. $^1\boldsymbol{J}_{C\alpha C\beta}$ values were obtained for 171 residues in the aligned sample, ranging from 26.1 to 43.5 Hz, with an average $^1\boldsymbol{J}_{C\alpha C\beta}$ of $34.9 \pm 3.7$ Hz. $^1D_{C\alpha C\beta}$ values were calculated for 165 residues in apo-MBP ranging from $-6.4$ (Phe 92) to 5.1 Hz (Ala 21). The mean experimental uncertainties were 0.07 and 0.13 Hz for couplings measured without ($^1J_{C\alpha C\beta}$) and with ($^1\boldsymbol{J}_{C\alpha C\beta}$) phage, resulting in an average uncertainty of 0.15 Hz for the dipolar coupling values.

**3D $^1D_{C\alpha C\beta}$-HN(CO)CA Method.** $^1D_{C\alpha C\beta}$ values can also be measured from a frequency domain approach, using the pulse sequence illustrated in Figure 1a, with the bracketed section replaced by Figure 1b. In this experiment magnetization is transferred from the $^1HN$ of residue $i$ to the $^{13}C^{\alpha}$ of residue $(i-1)$, as before. However, in the present scheme evolution from both $^{13}C^{\alpha}$ chemical shift and $^1\boldsymbol{J}_{C\alpha C\beta}$ coupling is recorded during the $t_1$ period (see below) so that the $^{13}C^{\alpha}-^{13}C^{\beta}$ coupling (residue $i-1$) is measured directly from the doublet splitting in $F_1$, while the $^{15}N$ and $^1HN$ chemical shifts of residue $i$ are recorded during $t_2$ and $t_3$, respectively. Sections from $F_1-F_3$ planes of 3D data sets recorded without (above) and with (below) phage are shown in Figure 2, with cross-peaks from residues Leu 139 (a) and Thr 249 (b) illustrated. $^1D_{C\alpha C\beta}$ values of $-5.5$ and 4.3 Hz are obtained for Leu 139 and Thr 249, in good agreement with couplings measured by using the 2D approach described above.

The sequence of Figure 1 makes use of accordion spectroscopy[42] to extend the period during which the $^{13}C^{\alpha}-^{13}C^{\beta}$ couplings evolve. Thus, although the $^{13}C^{\alpha}$ chemical shift proceeds for a period $t_1$, the $^1\boldsymbol{J}_{C\alpha C\beta}$ coupling is active for $(1+\kappa)t_1 + T$, with $T = pw_{C\alpha}^{180^\circ} + pw_{CO}^{180^\circ} + \Gamma pw_{c\alpha}^{90^\circ} + \lambda$, where $pw_{CO}^{180^\circ}$ is the selective $^{13}CO$ 180° pulse width and $\lambda$ is a delay equal to $pw_{CO}^{180^\circ}$ to compensate for $^{13}C^{\alpha}$ chemical shift evolution during this selective pulse. Note that the $^{13}CO$ and $^{15}N$ pulses in the middle of $t_1$ are applied simultaneously, with $pw_{CO}^{180^\circ} > pw_N^{180^\circ}$. The $^1H$ 180° pulse in the center of the $t_1$ period refocuses evolution arising from the two- and three-bond $^1HN-^{13}C^{\alpha}$ couplings. Evolution due to the two-bond $^1HN-^{13}C^{\alpha}$ coupling ($^1HN$ and $^{13}C^{\alpha}$ of residue $i-1$) during $t_1$ leads to an unresolved doublet in $F_1$, decreasing sensitivity. This is especially the case for the aligned sample where $^2D_{HNCA}$ can be substantial. In contrast, evolution from the three-bond $^1HN-^{13}C^{\alpha}$ coupling ($^1HN$ of residue $i$, $^{13}C^{\alpha}$ of residue $i-1$) does not complicate the $F_1$ multiplet structure since the TROSY approach is employed which selects only one of the two $^1HN$ spin states of residue $i$. The additional $^1H$ pulse applied prior to gradient 6 ensures that the correct TROSY component is ultimately selected. A product-operator description[43] shows that the signal of interest is modulated by the factor

$$\cos\{\pi^1 \boldsymbol{J}_{C\alpha C\beta}[(1+\kappa)t_1 + T]\} \exp(i\omega_{C\alpha} t_1) \exp\left(-\frac{t_1}{T_2^{eff,C\alpha}}\right) \qquad (3)$$

where $\omega_{C\alpha}$ is the $^{13}C^{\alpha}$ chemical shift and $T_2^{eff,C\alpha} = T_2^{C\alpha}/(1+\kappa)$,

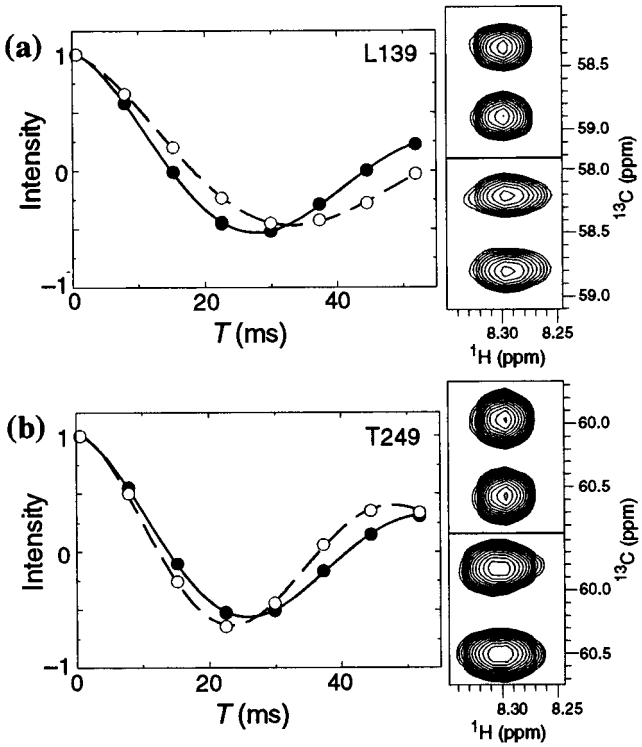


**Figure 2.** Measurement of $^1\boldsymbol{J}_{C\alpha C\beta}$ in $^{13}C,^{15}N,^2H$-labeled apo-MBP, 37 °C, pH 7.2, 600 MHz. Data are shown for residues L139 (a) and T249 (b). The left panels in (a) and (b) show the normalized intensities of cross-peaks obtained from spectra recorded in isotropic media (filled circles, 1.4 mM MBP) and phage solution (open circles, 1.1 mM MBP) using the 2D approach as a function of $T = 2T_C + pw_{C\alpha}^{180^\circ} + \Gamma pw_{C\alpha}^{90^\circ}$ (see Figure 1 and text for details). The solid and dashed lines are the nonlinear fits to the experimental data with use of eq 2. The upper and lower right panels show selected 2D slices from 3D spectra recorded of protein dissolved in isotropic and anisotropic media, respectively, presenting the multiplet components of each cross-peak. The splitting is approximately equal to $(\kappa+1)^1\boldsymbol{J}_{C\alpha C\beta}$, where $\kappa = 1.4$ (see text for further details).

(40) Logan, T. M.; Olejniczak, E. T.; Xu, R. X.; Fesik, S. W. *J. Biomol. NMR* **1993**, *3*, 225−231.
(41) Grzesiek, S.; Bax, A. *J. Biomol. NMR* **1993**, *3*, 185−204.
(42) Bodenhausen, G.; Ernst, R. R. *J. Magn. Reson.* **1981**, *45*, 367−373.
(43) Sorensen, O. W.; Eich, G. W.; Levitt, M. H.; Bodenhausen, G.; Ernst, R. R. *Prog. NMR Spectrosc.* **1983**, *16*, 163−192.

with $T_2^{C\alpha}$ the effective transverse relaxation time of the magnetization during each of the $t_1/2$ periods. The use of accordion spectroscopy increases, therefore, both the effective $^{13}C^{\alpha}-^{13}C^{\beta}$ coupling and the transverse relaxation rate by a factor of $(1 + \kappa)$. The nonzero value of $T$ ($T \sim 0.9$ ms) in eq 3 gives rise to antiphase dispersive contributions to the $F_1$ line shape. These "extra" dispersive lines lead to a (small) systematic overestimation of $^1\boldsymbol{J}_{C\alpha C\beta}$ values when couplings are estimated by the difference in peak positions of the doublet components.

To estimate the contributions from the dispersive lines to the measured couplings we have generated synthetic time domain data as a function of $^1\boldsymbol{J}_{C\alpha C\beta}$ and $T_2^{C\alpha}$ using eq 3 (program available from the authors upon request). The acquisition times ($t_1^{max} = 27.4$ ms) and processing parameters used in producing the synthetic 2D data sets were identical with the experimental values (see Materials and Methods). A value of $\kappa = 1.4$ was used in experiment and simulations as a compromise between the desired increase in doublet splittings and the concomitant decrease in sensitivity. Figure 3a illustrates the relation between "true" $^1\boldsymbol{J}_{C\alpha C\beta}$ values entered into the simulations and measured couplings extracted from the frequency difference of the doublet components for $T_2^{C\alpha}$ values of 33 (filled circles) and 100 ms (open squares). For values of $T_2^{C\alpha}$ ranging from 33 to 100 ms the correlation between actual and measured $^1\boldsymbol{J}_{C\alpha C\beta}$ values was found to be linear to excellent approximation, as shown in Figure 3a. Thus, it is straightforward to correct measured coupling values by using the simple relation, $\boldsymbol{J}_{C\alpha C\beta}^{Correct} = m\boldsymbol{J}_{C\alpha C\beta}^{Measured} + b$, where $m$ and $b$ are functions of $T_2^{C\alpha}$. Assuming that $^{13}C^{\alpha}$ line widths are insensitive to alignment,[18,21] $^1D_{C\alpha C\beta}$ values calculated from couplings measured by doublet splittings in spectra of unaligned and aligned samples can be corrected by multiplication with a line width-dependent correction factor ($m$ above), indicated in Figure 3b. Note that the correction factor levels off at approximately 0.96 and not 1 due to the short acquisition time employed (27.4 ms), leading to residual broadening of peaks.

In the case of apo-MBP all $^1D_{C\alpha C\beta}$ values have been corrected by using a factor of 0.936 that corresponds to a mean $T_2^{C\alpha}$ value of 47 ms, estimated from fitting the 2D data to eq 1, see above. Use of a constant correction factor is estimated to introduce errors of less than 3% for residues with $T_2^{C\alpha} = 33-64$ ms (Figure 3b), corresponding to more than 96% of the amino acids in apo-MBP. It is noteworthy that for $T_2^{C\alpha}$ values greater than 30 ms, corresponding to proteins with correlation times $\leq\sim$ 28 ns (deuterated protein), correction factors range from 0.89 ($T_2^{C\alpha} = 30$ ms) to 0.96. Because the dependence of the correction factor on molecular weight is quite small, it is possible to estimate correction factors without recording additional experiments from the approximate relation based on data from MBP, $T_{2,U}^{C\alpha} = (41000/MW_U)T_{2,MBP}^{C\alpha} = 1930/MW_U$, where $T_{2,U}^{C\alpha}$ is the estimated mean $T_2^{C\alpha}$ value (seconds) for the protein under study with molecular weight, $MW_U$. Alternatively, in cases where it is anticipated that relaxation times will vary significantly between different sites in the protein, $T_{2,U}^{C\alpha}$ can be determined experimentally by using the 2D pulse scheme of Figure 1 by recording spectra of protein without alignment using values of $T_c = 0$, $(1/2^1J_{C\alpha C\beta})$ $[1/T_2^{C\alpha} = -(1/^1J_{C\alpha C\beta})$ ln $(I[T_C{=}1/2^1J_{C\alpha C\beta}]/I[T_C{=}0])$, where $I$ is a peak intensity] and correction factors estimated from the experimental data. In general, however, factors obtained from the simple formula above are sufficient, especially considering that the corrections to the dipolar couplings are on the order of or less than the uncertainties in the measurements themselves (see below).

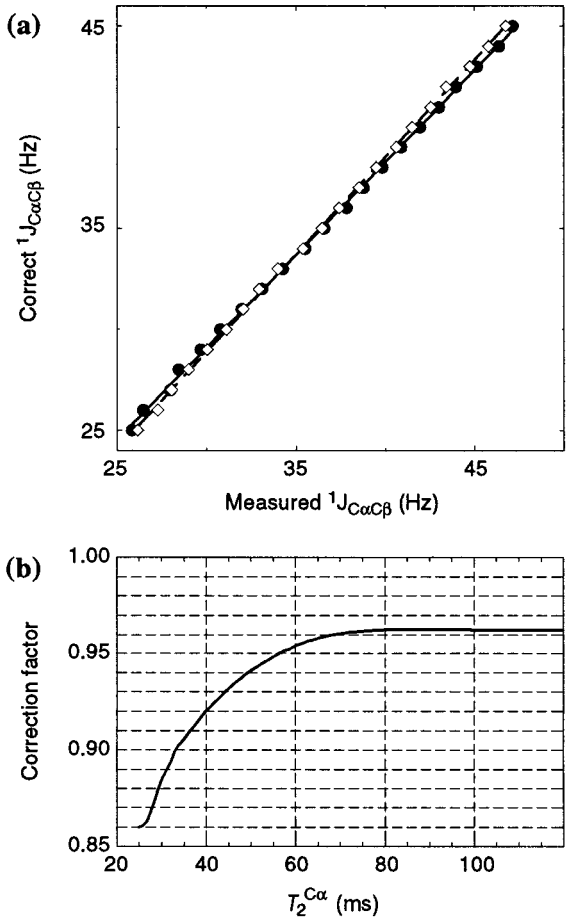


**Figure 3.** Effects of dispersive $F_1$ line shape contributions on $^1\boldsymbol{J}_{C\alpha C\beta}$ values measured from differences in peak doublet positions (3D accordion method). Synthetic data were generated by using experimental acquisition and spectral processing parameters for values of $^1\boldsymbol{J}_{C\alpha C\beta} =$ 25−45 Hz and $T_2^{C\alpha} = 25-200$ ms. (a) Correct vs measured $^1\boldsymbol{J}_{C\alpha C\beta}$ values for $T_2^{C\alpha} = 33$ ms (filled circles) and $T_2^{C\alpha} = 100$ ms (open squares). Solid and dashed lines indicate the linear regression results, $^1\boldsymbol{J}_{C\alpha C\beta}$(correct) $= m^1\boldsymbol{J}_{C\alpha C\beta}$(measured from $F_1$ peak separation) $+ b$, where $(m,b) = (0.914, 1.68$ Hz) for $T_2^{C\alpha} = 33$ ms and $(m,b) = (0.962, 0.03$ Hz) for $T_2^{C\alpha} = 100$ ms. The regression coefficients are 0.9996 and 0.9998, respectively. (b) The correction factors for the $^1D_{C\alpha C\beta}$ values as a function of $T_2^{C\alpha}$. These factors are strongly dependent on acquisition time and spectral processing parameters (see Materials and Methods). Note that these correction values are obtained by using pulse widths optimal for spectra recorded at 600 MHz. Since similar carbonyl (phase $\phi 7$, Figure 1) and $^{13}C^{\alpha}$ 180° (phase $\phi 2$) pulse widths can be used for data recorded at 500 MHz, the correction factors would be very similar to those reported here. Simulations establish that for data recorded at 800 MHz with the carbon pulses scaled by 6/8, correction factors range from approximately 0.91 ($T_2^{C\alpha} = 30$ ms) to 0.97 ($T_2^{C\alpha} =$ 100 ms).

The uncertainty in measured dipolar coupling values obtained by using the 3D method was estimated by performing repeat measurements of $^1\boldsymbol{J}_{C\alpha C\beta}$ with the oriented sample. The pairwise root-mean-squared deviation (rmsd) in $^1\boldsymbol{J}_{C\alpha C\beta}$ values is 0.5 Hz, corresponding to an uncertainty of 0.36 Hz in measured values. Assuming a similar level of precision in data obtained from the unoriented protein, an uncertainty of 0.5 Hz in $^1D_{C\alpha C\beta}$ values is expected. This is likely to be a slight overestimate since the quality of spectra recorded without phage is superior to the corresponding data sets obtained for the oriented sample, largely the result of residual $^1HN-^1HN$ dipolar couplings in the phage sample. The 3-fold decrease in precision relative to the 2D data

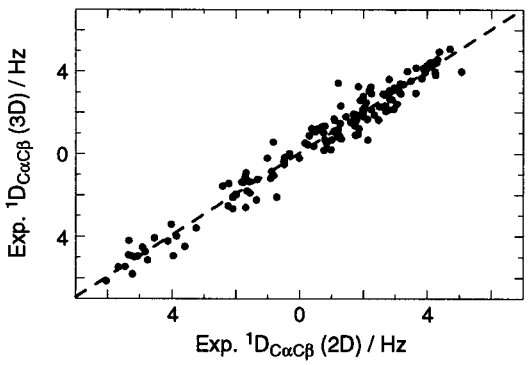


**Figure 4.** Comparison of $^1D_{C\alpha C\beta}$ coupling values for apo-MBP derived from the 2D and 3D methods. Errors introduced from the dispersive contributions to the $C^{\alpha}$ line shape (3D approach) have been corrected by multiplication of $^1D_{C\alpha C\beta}$ values by 0.936, as described in the text. The best-fit line to the data (indicated with dashes) has a slope and intercept of 0.997 and 0.06 Hz, respectively. The regression coefficient is 0.98.

and the extra work associated with correcting the measured couplings is compensated to some extent by the increased number of dipolar couplings that could be obtained with the 3D approach (240 vs 165).

$^1D_{C\alpha C\beta}$ couplings have also been measured on MBP by using a non-accordion based HN(CO)CA scheme described previously in connection with studies of ubiquitin.[27,28] For applications involving large proteins we prefer the accordion experiment described here, since the doublet components are significantly better resolved in this experiment.

Figure 4 shows a good correlation between $^1D_{C\alpha C\beta}$ values obtained from the 2D and 3D (corrected) methods described above. The slope and intercept of the best-fit line (dashed line in the figure) are 0.997 and 0.06 Hz, respectively, and the pairwise rmsd between values obtained from the two methods is 0.56 Hz, consistent with the errors in the data (see above).

**Comparison of Experimental and Predicted $^1D_{C\alpha C\beta}$ Values.** One of the important uses of dipolar couplings has been in reorienting domains of multidomain proteins, starting from a model where the intradomain structure is assumed to be correct.[20,44,45] Recently we have used a large number of dipolar couplings obtained from MBP in complex with $\beta$-cyclodextrin to compare the relative orientation of the N- and C-domains in solution vs the X-ray state. Of interest, substantial differences were observed between solution and X-ray conformations, with the solution structure related to the crystal structure by an 11° domain closure.[29] Domain orientation in MBP is of particular importance since the existence of open and closed forms for the molecule is thought to be crucial for its role in the signal transduction cascade that regulates both maltodextrin uptake and chemotaxis.[46] Binding of maltose to MBP induces an open to closed conformational change that subsequently facilitates binding to a number of chemoreceptors. It is of considerable interest, therefore, to extend our previous studies to examine domain orientation in ligand-free MBP. In this regard we have compared experimental $^1D_{C\alpha C\beta}$ values with those predicted from the X-ray structure of apo-MBP (pdb accession code 1omp[47]), in which the two domains of MBP adopt an "open" conformation, and with couplings predicted by the maltotetraose-bound state of the protein (pdb accession code 4mbp[48]) representing the "closed" conformation (closure of domains ~35° relative to orientation in 1omp).

Figures 5a and 5b illustrate the excellent agreement obtained for $^1D_{C\alpha C\beta}$ values measured by the 2D and 3D methods, respectively, with those predicted from the apo-MBP crystal structure. Experimental data have been used only for those residues within either the N- or C-domain (i.e., excluding residues from the linker region), corresponding to 159 and 225 values for the 2D and 3D data sets. Alignment parameters used in the prediction of the dipolar couplings were obtained by using the experimental $^1D_{C\alpha C\beta}$ values, the X-ray coordinates, and our software, Conformist1.0.[29] The pairwise rmsd between experimental and calculated $^1D_{C\alpha C\beta}$ values are 0.55 and 0.69 Hz for the 2D- and 3D-derived data sets, respectively. We have investigated whether the fits would improve by allowing the domains to reorient using a target function that minimizes the difference between measured and predicted dipolar couplings, as described by Skrynnikov et al. previously.[29] The resulting domain orientation was essentially unchanged from the 1omp structure, with F-tests[49] verifying that the improvement in the fit was not statistically significant at even the 75% confidence level.

In contrast to the excellent correlation between experimental and predicted $^1D_{C\alpha C\beta}$ values with use of the 1omp structure, a much poorer level of agreement was obtained when the structure of maltotetraose-bound MBP (4mbp) was employed, Figures 5c,d, prior to domain reorientation. Subsequent rigid body rotation of the domains of the 4mbp structure with the $^{13}C^{\alpha}-^{13}C^{\beta}$ dipolar couplings resulted in structures that are very similar to the 1omp coordinate set (less than 1° difference in domain closure between the dipolar coupling refined 4mbp structures and 1omp). Not surprisingly, the agreement between measured and predicted $^1D_{C\alpha C\beta}$ dipolar coupling values improves considerably when the domains are allowed to reorient, with pairwise rmsds dropping from 1.62 to 0.68 Hz for values obtained from the 2D method and from 1.58 to 0.80 Hz for couplings measured with the 3D approach. The domain reorientation analysis described presently has also been repeated by using the uncorrected $^1D_{C\alpha C\beta}$ dipolar coupling values from the 3D data set to establish whether correction of these couplings (as described above) is essential in practical applications. Since the correction only scales the couplings uniformly, no difference in relative domain orientations would be obtained when either corrected or uncorrected $^{13}C^{\alpha}-^{13}C^{\beta}$ couplings are employed exclusively; therefore both $^{13}C^{\alpha}-^{13}C^{\beta}$ and $^{13}C^{\alpha}-^{13}CO$ couplings

(44) Fischer, M. W.; Losonczi, J. A.; Weaver, J. L.; Prestegard, J. H. *Biochemistry* **1999**, *38*, 9013−22.
(45) Losonczi, J. A.; Andrec, M.; Fischer, M. W.; Prestegard, J. H. *J. Magn. Reson.* **1999**, *138*, 334−42.
(46) Mowbray, S. L.; Sandgren, M. O. *J. Struct. Biol.* **1998**, *124*, 257−75.
(47) Sharff, A. J.; Rodseth, L. E.; Spurlino, J. C.; Quiocho, F. A. *Biochemistry* **1992**, *31*, 10657−10663.
(48) Quiocho, F.; Spurlino, J.; Rodseth, L. *Structure* **1997**, *5*, 997−1015.
(49) Bevington, P. R.; Robinson, D. K. *Data Reduction and Error Analysis for the Physical Sciences*; WCB/McGraw-Hill: New York, 1992.
(50) Freeman, R.; Kempsell, S. P.; Levitt, M. H. *J. Magn. Reson.* **1980**, *38*, 453−479.
(51) Kay, L. E.; Ikura, M.; Tschudin, R.; Bax, A. *J. Magn. Reson.* **1990**, *89*, 496−514.
(52) Geen, H.; Freeman, R. *J. Magn. Reson.* **1991**, *93*, 93−141.
(53) McCoy, M. A.; Mueller, L. *J. Am. Chem. Soc.* **1992**, *114*, 2108−2112.
(54) McCoy, M. A.; Mueller, L. *J. Magn. Reson.* **1992**, *98*, 674−679.
(55) Shaka, A. J.; Keeler, J.; Frenkiel, T.; Freeman, R. *J. Magn. Reson.* **1983**, *52*, 335−338.
(56) Vuister, G. W.; Bax, A. *J. Magn. Reson.* **1992**, *98*, 428−435.
(57) Boyd, J.; Soffe, N. *J. Magn. Reson.* **1989**, *85*, 406−413.
(58) Patt, S. L. *J. Magn. Reson.* **1992**, *96*, 94−102.
(59) Marion, D.; Ikura, M.; Tschudin, R.; Bax, A. *J. Magn. Reson.* **1989**, *85*, 393−399.
(60) Kay, L. E.; Keifer, P.; Saarinen, T. *J. Am. Chem. Soc.* **1992**, *114*, 10663−10665.
(61) Schleucher, J.; Sattler, M.; Griesinger, C. *Angew. Chem., Int. Ed. Engl.* **1993**, *32*, 1489−1491.

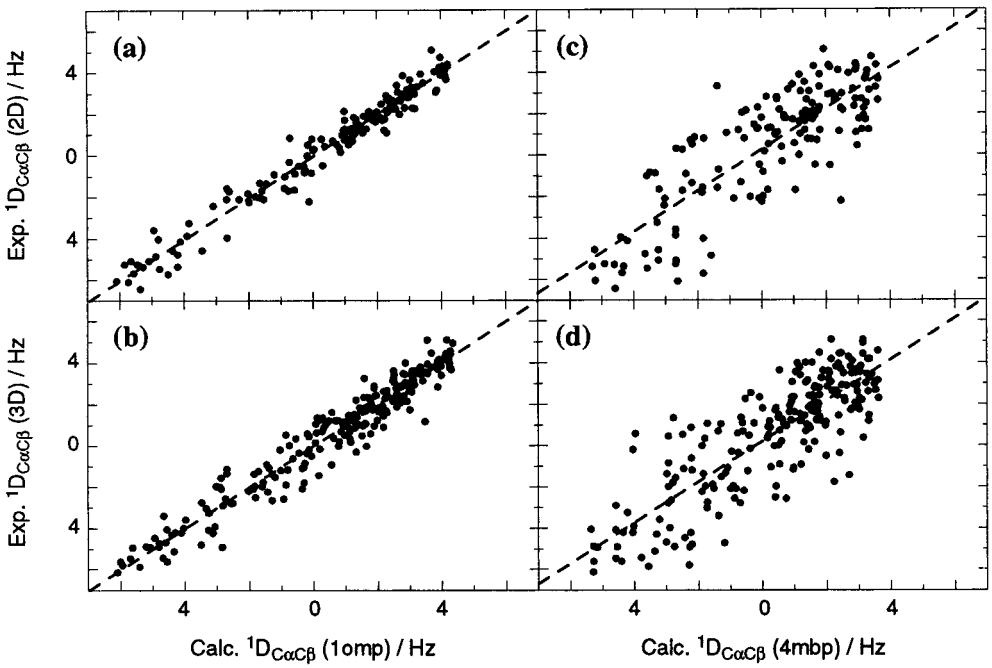


**Figure 5.** Comparison of experimental $^{13}C^{\alpha}-^{13}C^{\beta}$ dipolar couplings with those predicted with use of the X-ray crystal structures of apo-MBP[47] (1omp.pdb, open conformation) and maltotetraose-bound MBP[48] (4mbp.pdb, closed conformation). Alignment frames were calculated from the $^{13}C^{\alpha}-^{13}C^{\beta}$ couplings by using the in-house written software Conformist1.0.[29] All available $^1D_{C\alpha C\beta}$ values were included in the analysis except those from the residues linking the two domains, i.e. residues 1−5, 110−113, 259−263, and 310−315. The excellent agreement between experimental $^1D_{C\alpha C\beta}$ values and those obtained based on the apo-MBP X-ray structure (regression coefficients of 0.98 and 0.96, slopes of 1.0 and 1.0, and *y*-intercepts of −0.04 and −0.02 Hz for the 2D and 3D methods) indicate that very similar domain orientations are found in the solution and crystal states (a, b). The sensitivity of the $^1D_{C\alpha C\beta}$ data to domain orientation is indicated in panels (c) and (d) where experimental couplings measured for apo-MBP are compared with those predicted from a closed domain conformation, maltotetraose-bound MBP. Slopes of 0.99 and 0.99, *y*-intercepts of 0.25 and 0.21 Hz, and regression coefficients of 0.82 and 0.83 are obtained in (c) and (d), respectively.

were used. Equivalent relative domain orientations were obtained with both uncorrected and corrected $^1D_{C\alpha C\beta}$ values, indicating, not unexpectedly, that the effects of the errors in $^1D_{C\alpha C\beta}$ are small.

We have not been able to ascertain why significant differences in domain orientation are obtained between solution and crystal forms of the $\beta$-cyclodextrin-loaded molecule but not for apo-MBP. Both forms of the protein crystallize in the same space group (*P*1) and similar contacts are observed between adjacent molecules in the lattice. Clearly the differences in interdomain structure must arise from subtle effects. The fact that it may be difficult to predict from inspection of protein packing in the crystal lattice when domain orientation in solution and crystal forms will be different underscores the need for additional solution-based approaches to address this issue. In this regard, dipolar couplings are particularly powerful and can be easily used to "refine" high-resolution X-ray structures that may be influenced by the lattice environment.

In summary, two methods have been presented for measuring one-bond $^{13}C^{\alpha}-^{13}C^{\beta}$ dipolar couplings in high molecular weight, deuterated proteins, with a good correlation observed between couplings obtained by the two approaches. A comparison of $^1D_{C\alpha C\beta}$ values with those predicted from the X-ray structure of apo-MBP establishes that both intra- and interdomain structure are very similar in solution and crystal states.

**Acknowledgment.** The authors are grateful to Dr. Nikolai Skrynnikov for help with using the program Conformist1.0 and Professor James Rini and co-workers for help with visualizing MBP molecules in the crystal environment. The research was supported by a grant from the Medical Research Council of Canada. J.E. is a recipient of a postdoctoral fellowship from the Swedish Foundation for International Cooperation in Research and Higher Education (STINT). L.E.K is an International Howard Hughes Research Scholar. This paper is dedicated to the memory of the 1993 Chemistry Nobel Prize Laureate, Dr. Michael Smith, in appreciation of his efforts in recruiting one of us (L.E.K.) back to Canada after training in the U.S.A.

JA003833Y